

We are IntechOpen, the world's leading publisher of Open Access books Built by scientists, for scientists

5,500

Open access books available

136,000

International authors and editors

170M

Downloads

Our authors are among the

154

Countries delivered to

TOP 1%

most cited scientists

12.2%

Contributors from top 500 universities



WEB OF SCIENCE™

Selection of our books indexed in the Book Citation Index
in Web of Science™ Core Collection (BKCI)

Interested in publishing with us?
Contact book.department@intechopen.com

Numbers displayed above are based on latest data collected.
For more information visit www.intechopen.com



Wavelet Based Multicarrier Modulation (MCM) Systems: PAPR Analysis

Jamaluddin Zakaria and Mohd Fadzli Mohd Salleh

Abstract

Orthogonal frequency division multiplexing (OFDM) is a prominent system in transmitting multicarrier modulation (MCM) signals over selective fading channel. The system offers to attain a higher degree of bandwidth efficiency, higher data transmission, and robust to narrowband frequency interference. However, it incurs a high peak-to-average power ratio (PAPR) where the signals work in the nonlinear region of the high-power amplifier (HPA) results in poor performance. Besides, an attractive dynamic wavelet analysis and its derivatives such as wavelet packet transform (WPT) demonstrates almost the same criteria as the OFDM in MCM system. Wavelet surpasses Fourier based analysis by inherent flexibility in terms of windows function for non-stationary signal. In wavelet-based MCM systems (wavelet OFDM (WOFDM) and Wavelet packet OFDM (WP-OFDM)), the constructed orthogonal modulation signals behaves similar to the fast Fourier transform (FFT) does in the conventional OFDM (C-OFDM) system. With no cyclic prefix (CP) need to be applied, these orthogonal signals hold higher bandwidth efficiency. Hence, this chapter presents a comprehensive study on the manipulation of specified parameters using WP-OFDM, WOFDM and C-OFDM signals together with various wavelets under the additive white Gaussian noise (AWGN) channel.

Keywords: multicarrier modulation (MCM), orthogonal frequency division multiplexing (OFDM), peak-to-average power ratio (PAPR), wavelet transform, wavelet packet transform (WPT)

1. Introduction

Orthogonal Frequency Division Multiplexing (OFDM) technique provides a number of advantages: In OFDM since the subcarriers are overlapped, accomplishes a higher degree of spectral efficiency that results in higher transmission data rates. Considering the use of the efficient FFT technique, the process is considered computationally lower. Besides, in the Single-Carrier Modulation (SCM) the ISI problem which commonly occurs the use of the cyclic prefix (CP) greatly eliminates the problem [1]. The division of a channel into several narrowband flat fading (subchannels) results in the subchannels being more resilient towards frequency selective fading. The loss of any subcarrier(s) due to channel frequency selectivity, proper channel coding schemes can recover the lost data [1]. Thus, this technique

offers robust protection against channel impairments without the need to implement an equalizer as in the SCM, and this greatly reduces the overall system complexity. However, the high Peak-to-Average Power Ratio (PAPR) has been the major drawback in the OFDM system. This situation happens when the peak OFDM signals surpass the specified threshold and as a result the high-power amplifier (HPA) operates in a nonlinear region. This produces spectral regrowth of the OFDM signals and broken the orthogonality among the subcarriers. Thus, the effect on bit error rate (BER) performance at the receiver is poor.

To deliver massive high-speed data over a wireless channel, Multi-carrier-modulation (MCM) scheme has been widely used transmission technique. Despite its advantages, the MCM scheme is prone to high PAPR signal transmission, which has been single out as the main difficulty. In the MCM scheme, the conventional way to obtain orthogonal subcarrier signals is by using a Fourier transform. The emergence of wavelet transforms has paved the way for new promising techniques to obtain orthogonal subcarrier signals in future MCM systems. Wavelet transforms have been testified practical for the MCM system due to the orthogonal overlapping symbols property that they possess in time and frequency domains, respectively.

In order to mitigate PAPR, there have been many techniques proposed in literature either to reduce the peak power with fixed average power or alter the distribution so that the average power produced has smaller peak power [2–6]. Due to this, there are two categories of PAPR reduction techniques which are called as signal distortion technique and signal scrambling technique. A prominent technique known as Partial Transmit Sequence (PTS) has been first introduced in [7]. This technique categorized as signal scrambling offers big potential for further exploration as explored in the works [8–11].

This chapter presents the analysis of various wavelet families in their applicability towards MCM systems and their PAPR profiles. Details analysis is presented for obtaining the BER results for various Wavelets.

2. Background

2.1 Wavelet transform

In this section the basic concept of wavelet and wavelet packet transform (WPT) are presented. The WPT is constructed based on the continuous wavelet transform (CWT) and wavelet transform (WT) theory. For ease of reading, all the following equations in these subsections are mostly taken from [12–15].

2.1.1 Discrete wavelet transform (DWT)

The computation cost for wavelet coefficients in the CWT is high since they are highly redundant data, which is not desirable for real application. Therefore, discrete wavelets offer as the alternative for practical applications. In discrete wavelets, the scalable and translatable wavelets are discrete. The process of discrete scaling and translation of the mother wavelet can be expressed as

$$\psi_{\alpha,\beta} = \sqrt{a_0^\alpha} \psi(a_0^\alpha t - \beta_{b_0}) \quad (1)$$

where a_0 represents the fixed step of dilation and b_0 indicates the translation factor. The integer α and β signify the indices scale and translation, respectively. The scaling in time domain correlates with an inverse scaling in frequency domain,

therefore the product of $(\Delta t_{a,b}) (\Delta f_{a,b})$ is independent of the dilation parameter a . If any time resolution gain is obtained, this inversely effect the cost of frequency resolution and vice versa. Therefore, this detains the Heisenberg uncertainty principle for the dilated and translated wavelet $\psi_{CWT_{a,b}}(t)$ and the mother wavelet $\psi_{CWT}(t)$. The most natural choice for dilation step is 2 that results in octave bands or dyadic scales. The wavelet is compressed in frequency domain by a factor of 2 for each successive value of scale index. This produces the stretched in time domain by the same factor. The translation factor is set to the value of “1” to get the dyadic sampling fashion. The time-shift and scaling function are set as [16];

$$\varphi_\beta = \varphi(t - \beta), \beta \in Z, \varphi \in L^2 \quad (2)$$

where Z is the set of all integer numbers, and $L^2(\mathbb{R})$ is the vector space of square integrated function. The parameter v_0 is a space spanned by scaling function, which is defined as

$$v_0 = \overline{\text{Span}\{\varphi_\beta(t)\}}_{\beta}, \beta \in Z \quad (3)$$

In this subspace, if $x(t) \in v_0$, it can be expressed as

$$x(t) = \sum_{\beta=-\infty}^{+\infty} \alpha_\beta \varphi_\beta(t) \quad (4)$$

One can increase the size of the subspace by changing the time scale of the scaling functions. The two-dimensional parameterization (time and scale) of scaling function $\varphi(t)$ from v_0 to v_α can be expressed as

$$\varphi_{\alpha,\beta} = 2^{\alpha/2} \varphi(2^\alpha t - \beta) \quad (5)$$

Then, the new function for the expanded subspace v_α is given as

$$v_\alpha = \overline{\text{span}\{\varphi_\beta(2^\alpha t)\}}_{\beta} = \overline{\text{span}\{\varphi_{\alpha,\beta}(t)\}}_{\beta} \quad (6)$$

In the extended subspace, whenever $x(t) \in v_\alpha$, then it can be expressed as

$$x(t) = \sum_{\beta=-\infty}^{+\infty} \alpha_\beta \varphi(2^\alpha t + \beta) \quad (7)$$

From (Eq. (7)), the span v_α is larger than v_0 , for $\alpha > 0$ and $\varphi_{\alpha,\beta}(t)$ able to represent the finer detail (due to its finer scale). For $\alpha < 0$ this condition is true that represents for the coarse scale. Wavelet obeys to multi-resolution concept's requirement, where every signal is decomposed into finer detail gradually as expressed as [17, 18].

$$\dots C v_{-2} C v_{-1} C v_0 C v_1 C v_2 C \dots \quad (8)$$

where the terms $v_{+\infty} = L^2$, and $v_{-\infty} = \{0\}$ indicate that within the same vector space of L^2 , there exist both high resolution and low-resolution coefficients.

Consequently, if $x(t) \in v_a$, then $x(2t) \in v_{a+1}$. Additionally, the $\phi(t)$ term is expressed as the weighted sum of the time-shifted scaling function

$$\varphi(t) = \sum_{n=-\infty}^{+\infty} h(n)\sqrt{2}\varphi(2t - n), n \in Z \quad (9)$$

where the term $h(n)$ represents the scaling function coefficients (sequence of real or imaginary numbers). The $v_{\alpha+1}$ is the expanded space of v_α and w_α represents the corresponding orthogonal complement. Therefore, a new set of spaces is produced. Suppose that $w_{\alpha+1}$ be the subspace spanned by the wavelet, the enlargement of v_1 and v_2 space are written as (Eq. (10)) below and as illustrated as in **Figure 1** [19].

$$\begin{aligned} v_1 &= v_0 \oplus w_0 \\ v_2 &= v_1 \oplus w_1 = (v_0 \oplus w_0) \oplus w_1 \\ &\vdots \\ v_{\alpha+1} &= v_\alpha \oplus w_\alpha = v_0 \oplus_{l=0}^{\alpha} w_l, \forall \alpha \in Z \end{aligned} \quad (10)$$

The definition of the wavelet function $\psi(t)$ is the same as the scaling space v_0 . Let the space spanned by the wavelet function $\psi_\beta(t)$ be w_0 , and the expanded space spanned by $\psi_{\alpha,\beta}(t)$ be w_α that is obtained after using (Eq. (3)) to (Eq. (6)). The w_α term is orthogonal to v_α and thus the orthogonality between $\varphi(t)$ and $\psi(t)$ is given as [19];

$$\langle \varphi_{\alpha,\beta}(t), \psi_{\alpha,\beta}(t) \rangle = \int \varphi_{\alpha,\beta}(t)\psi_{\alpha,\beta}(t)dt = 0 \quad (11)$$

Due to these wavelets are in space spanned by the next finer scaling function, the wavelet function $\psi(t)$ can be expressed by the sum of the weighted time-shifted wavelet function given as

$$\psi(t) = \sum_{n=-\infty}^{+\infty} g(n)\sqrt{2}\varphi(2t - n), n \in Z \quad (12)$$

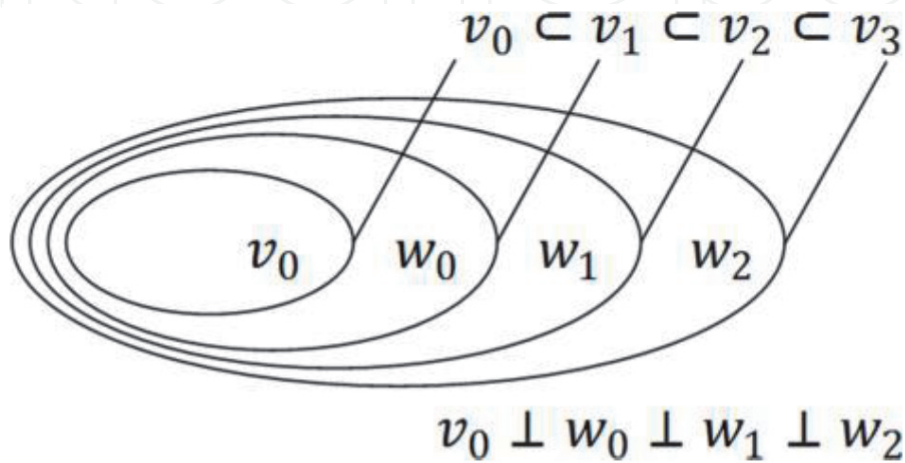


Figure 1.
Wavelet vector spaces and scaling function.

where $g(n)$ is called the wavelet function coefficient. The relationship between wavelet filter $g(n)$ and scaling filter $h(n)$ can be expressed as [19];

$$g(n) = (-1)^n h(1 - n) \quad (13)$$

Both coefficients are restricted by the orthogonality condition. If $h(n)$ has a finite even length N , then the (Eq. (13)) can be rewritten as

$$g(n) = (-1)^n h(N - 1 - n) \quad (14)$$

The wavelet function coefficients $g(n)$ is normally required by the orthonormal perfect reconstruction (PR) process. In the communication system point of view, this PR process offers advantage to the receiver whereby the received signals can be reconstructed perfectly. For example, Haar wavelet below is analyzed with the wavelet function $\psi(t)$ can be expressed as

$$\psi(t) = \begin{cases} 1 & 0 \leq t < 0.5 \\ -1 & 0.5 \leq t < 1 \\ 0 & \text{otherwise} \end{cases} \quad (15)$$

and its scaling function is

$$\varphi(t) = \begin{cases} 1 & 0 \leq t \leq 1 \\ 0 & \text{otherwise} \end{cases} \quad (16)$$

Furthermore, the basic version of Haar wavelet for wavelet and scaling function is shown in **Figure 2**.

The Haar filter coefficients are obtained by applying (Eq. (9)) and (Eq. (12)).

$$g(n) = \left(\frac{1}{\sqrt{2}}, \frac{-1}{\sqrt{2}} \right) \quad (17)$$

$$h(n) = \left(\frac{1}{\sqrt{2}}, \frac{1}{\sqrt{2}} \right) \quad (18)$$

Furthermore, the signal $x(t) \in L^2(\mathbb{R})$ has its discrete wavelet expansion given as [14].

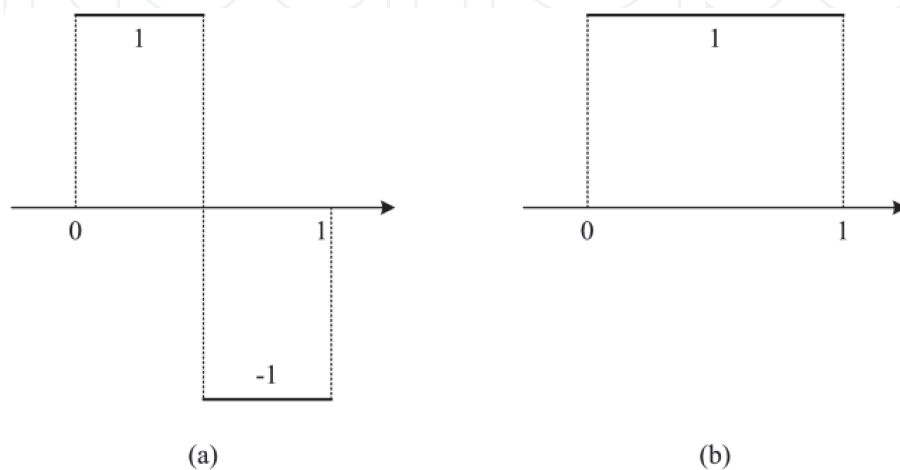


Figure 2.
 Haar Wavelet transform (a) mother wavelet function, (b) scaling function.

$$x(t) = \sum_{\beta=-\infty}^{+\infty} c_{\alpha_0}(\beta) \varphi_{\alpha_0, \beta}(t) + \sum_{\beta=-\infty}^{+\infty} \sum_{\alpha=\alpha_0}^{+\infty} d_{\alpha}(\beta) \psi_{\alpha, \beta}(t) \quad (19)$$

where $\alpha, \beta, \in Z$ which Z is real integer. The α_0 is an arbitrary integer, and $L^2(\mathbb{R})$ is the vector space of the square integrated function. The frequency (or scale) and time localizations are provided by the parameters α and β respectively. The approximation coefficient and the detail coefficient have been deduced as $c_{\alpha}(\beta)$ and $d_{\alpha}(\beta)$ respectively.

In the wavelet expansion, by manipulating (Eq. (9)) and (Eq. (19)), the higher scale (i.e. $\alpha + 1$) can also be obtained that results the approximation coefficient as

$$c_{\alpha}(\beta) = \langle x(t), \varphi_{\alpha, \beta}(t) \rangle = \int x(t) 2^{\alpha/2} \varphi(2^{\alpha}t - \beta) dt = \sum_m h(m - 2\beta) c_{\alpha+1}(m) \quad (20)$$

while the detail coefficient is expressed as

$$d_{\alpha}(\beta) = \langle x(t), \psi_{\alpha, \beta}(t) \rangle = \int x(t) 2^{\alpha/2} \psi(2^{\alpha}t - \beta) dt = \sum_m g(m - 2\beta) c_{\alpha+1}(m) \quad (21)$$

Both the terms of $c_{\alpha}(\beta)$ and $d_{\alpha}(\beta)$ in (Eq. (20) and (21)) are computed by taking the weighted sum of DWT coefficients of higher scale ($\alpha + 1$). In order to obtain the scaling of the DWT coefficients ($c_{\alpha}(\beta)$) at scale α , the scaling function coefficient $h(n)$ is convolved with the scaling DWT coefficients ($c_{\alpha+1}(\beta)$) at scale $\alpha + 1$, followed by subsampling with a factor of 2. Similarly, to obtain the wavelet DWT coefficients ($d_{\alpha}(\beta)$) at scale α , the wavelet function coefficient $g(n)$ is convolved with the scaling DWT coefficients ($c_{\alpha+1}(\beta)$) at scale $\alpha + 1$, followed by subsampling with a factor of 2. Hence, as shown in **Figure 3**, that both of these expressions can be illustrated as 2-channel filter banks analysis [20].

The input signal to the 2-channel filter bank is split into two parts. The first portion of the signal goes to filter H and second goes to filter G . Subsequently, both the filtered signals are subsampled by 2. Each filtered signal contains half of the number of original samples and spans half of the frequency band. However, the number of samples at the output of the filter bank is the same as the original signal since there are two filters used. The decomposition process starts at the largest scale of $c(\beta)$. If there are three level of decompositions involved, this implies the term $c_3(\beta)$ exist and produces the terms $c_0(\beta)$, $d_0(\beta)$, $d_1(\beta)$ and $d_2(\beta)$ at the decomposition branches, as illustrated in **Figure 4**.

On the other hand, the reconstruction of the DWT coefficients process is expressed by (Eq. (19)). If (Eq. (9)) (for scaling refinement) and (Eq. (12))

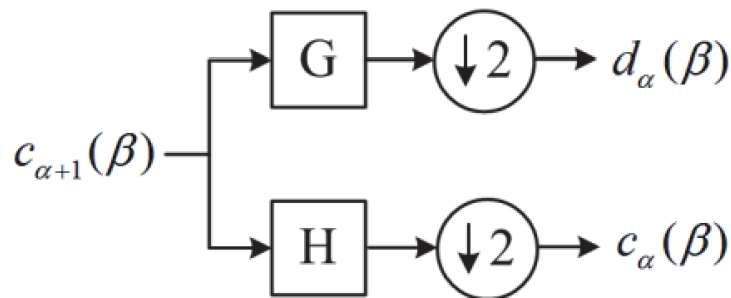


Figure 3.
DWT decomposition (single level).

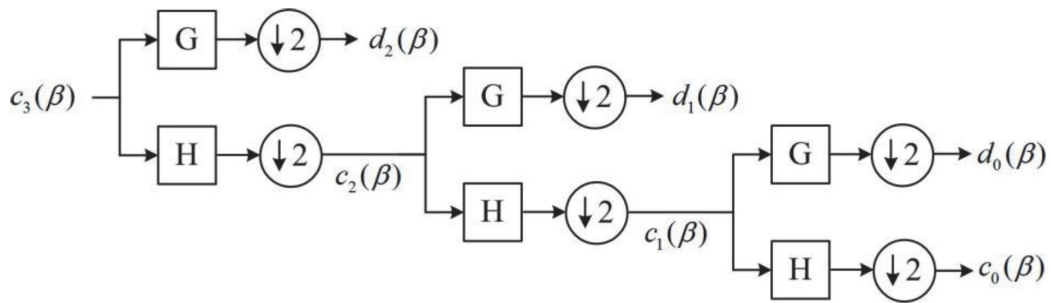


Figure 4.
 DWT decomposition (three level).

(wavelet function) are substituted into (Eq. (19)) (reconstruction function), thus produces

$$\begin{aligned}
 x(t) &= \sum_{\beta=-\infty}^{+\infty} c_{\alpha_0}(\beta) \varphi_{\alpha_0, \beta}(t) + \sum_{\beta=-\infty}^{+\infty} \sum_{\alpha=\alpha_0}^{+\infty} d_{\alpha}(\beta) \psi_{\alpha, \beta}(t) \\
 &= \sum_{\beta=-\infty}^{+\infty} c_{\alpha_0}(\beta) \sum_{n=-\infty}^{+\infty} h(n) (\sqrt{2})^{\alpha+1} \varphi(2^{\alpha+1} - 2\beta - n) \\
 &\quad + \sum_{\beta=-\infty}^{+\infty} \sum_{\alpha=-\infty}^{+\infty} d_{\alpha}(\beta) \sum_{n=-\infty}^{+\infty} g(n) (\sqrt{2})^{\alpha+1} \varphi(2^{\alpha+1} - 2\beta - n) \quad (22)
 \end{aligned}$$

By multiplying both sides of (Eq. (22)) with $\varphi(2^{\alpha+1} - \beta)$ and taking the integral produces the lower scale of DWT coefficients [18], the scaling DWT coefficients of higher scale is given as

$$c_{\alpha+1}(\beta) = \sum_m c_{\alpha}(m) h(\beta - 2m) + \sum_m d_{\alpha}(m) g(\beta - 2m) \quad (23)$$

This implies that the scaling DWT coefficients at a certain value $(\alpha + 1)$ can be computed by taking the weighted sum of wavelet DWT coefficients that are multiplied with the scaling DWT coefficients at scale α . **Figure 5** illustrates this process which is known as a 2-channel synthesis filter bank. The scaling DWT coefficients $(c_{\alpha}(\beta))$ and wavelet DWT coefficients $(d_{\alpha}(\beta))$ at scale α are first up-sampled by factor 2. Then, the scaling DWT coefficients $(c_{\alpha}(\beta))$ are filtered with a LPF \hat{H} , and the wavelet DWT coefficients $(d_{\alpha}(\beta))$ are filtered with a HPF \hat{G} respectively. Finally, the two filtered signals are added together to form the scaling DWT coefficients at scale $\alpha + 1$ i.e. $(c_{\alpha+1}(\beta))$.

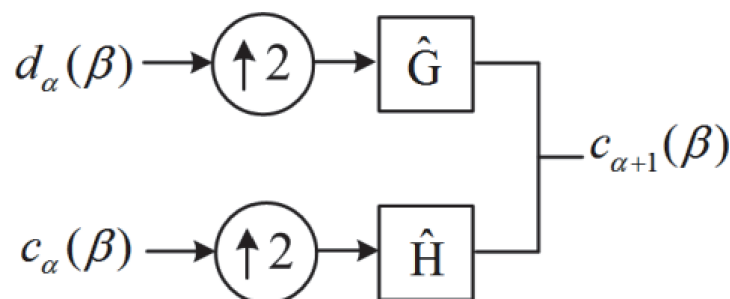


Figure 5.
 DWT reconstruction (single level).

In short, the DWT decomposes signals into coefficients. The IDWT reconstructs the original signals from coefficients which can be implemented efficiently by iterating the 2-channel synthesis filter bank.

2.1.2 Wavelet packet transform (WPT)

In DWT decomposition, the direction of decomposition is heading towards the low pass branches, i.e. the sequence of iteration for the 2-channel filter bank is always taking the low pass filters. At the end of decomposition, the low frequencies portion contains fewer numbers of coefficients, hence occupying a narrow bandwidth. The high frequencies portion contains larger number of coefficients, hence occupying a wide bandwidth.

On the other hand, wavelet packet transform (WPT) executes the iteration of 2-channel filter bank on both sides, i.e. on the low pass and high pass filter branches for decomposition. Therefore, the WPT has evenly space frequency resolution and similar bandwidth size since both the high frequency and low frequencies components are decomposed. In WPT, the filter bank structure is expanded into a full binary tree. A set of WPT coefficients is labeled by ζ and the level that corresponds to the depth a node in the tree structure is indicated by l and parameter p indicates the position at current node. Every parent node is split by the WPT in two orthogonal subspaces W_l^p which is located at the next recursive level, and is given as [19];

$$W_l^p = W_{l+1}^{2p} \oplus W_{l+1}^{2p+1}, W_l^p = \overline{\text{Span}\{2^{l/2}\zeta_l^p(2^l t - \beta)\}} \quad (24)$$

In WPT, the scaling WPT coefficients are denoted as ζ_{l+1}^{2p} and wavelet WPT coefficients are labeled as ζ_{l+1}^{2p+1} , given as in the following expressions, and are depicted as in **Figure 6**.

$$\zeta_{l+1}^{2p}(\beta) = \sum_m h(m - 2\beta)\zeta_l^p(m) \quad (25)$$

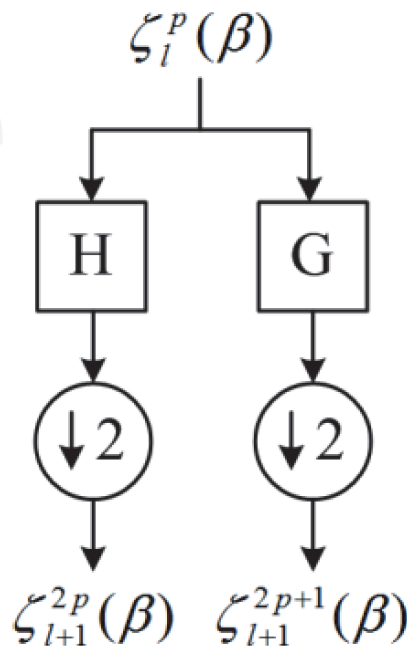


Figure 6.
WPT decomposition at single level.

$$\zeta_{l+1}^{2p+1}(\beta) = \sum_m g(m - 2\beta) \zeta_l^p(m) \quad (26)$$

In WPT, the number of iterations by the 2-channel filter bank increases exponentially as the number of levels increased. Therefore, WPT has higher computational complexity than the regular DWT. The WPT requires $O(N \log(N))$ operation (by using fast filter bank algorithm), while Fast Fourier Transform (FFT) requires only $O(N)$ operations to complete DWT [16]. The reconstruction (inverse WPT) is executed by taking the reverse direction of the tree in **Figure 6**. The wavelet packet coefficients $\zeta_l^p(\beta)$ at any level l can be expressed as

$$\zeta_l^p(\beta) = \sum \zeta_{l+1}^{2p}(m) h(\beta - 2m) + \sum \zeta_{l+1}^{2p+1}(m) g(\beta - 2m) \quad (27)$$

2.2 Multicarrier modulation (MCM) system

Multicarrier modulation (MCM) scheme is a technique that transforms the high-speed serial signals into multiple low-speed parallel signals with N overlapping subcarriers. This special multicarrier modulation scheme was introduced by Chang [21], and is known as the orthogonal frequency division multiplexing (OFDM). The technique is widely used in various applications such as in European Digital Audio Broadcasting (DAB), IEEE 802.11 (WiFi) and IEEE 802.16 (WiMAX). OFDM has high spectral efficiency and consecutive subcarriers experience no crosstalk if the orthogonality is preserved.

In this study two wavelet-based MCM systems are used i.e. the wavelet-based OFDM (WOFDM) and wavelet packet-based OFDM (WP-OFDM) systems. As seen above. The primary difference between these two MCM systems is the way the wavelet tree being expanded. Therefore, in wavelet-based OFDM (WOFDM), the decomposition process expands the branches in dyadic way. In wavelet packet-based OFDM (WP-OFDM), the decomposition process expands the nodes as a full binary tree. Hence, wavelet packet process possesses richer signal analysis than wavelets process and for the detail analysis, wavelet packet process is capable to focus on any of the tree nodes. This main difference of the two MCM systems is illustrated in **Figure 7**. Notice that the wavelet decomposition produces different range of bandwidth divisions. The wavelet bandwidth is in form of dyadic division, while wavelet packet bandwidth is uniform. Therefore, the use of wavelet packet

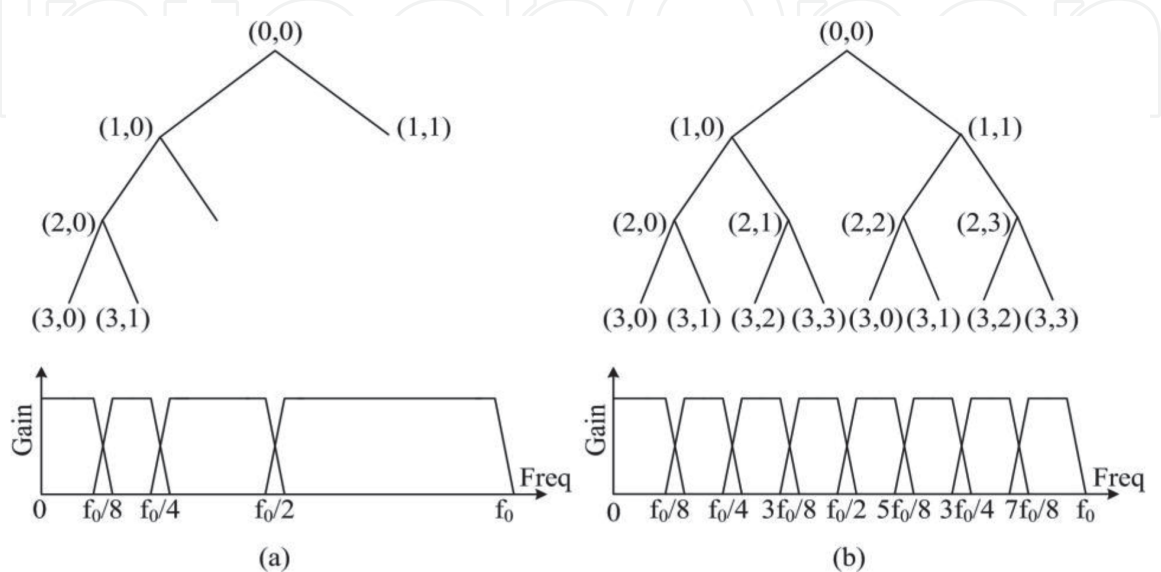


Figure 7.
 Decomposition and bandwidth division for (a) DWT and (b) WPT.

transform in MCM system is preferable since its major characteristic resembles the conventional OFDM [22].

In wavelet packet-based OFDM (WP-OFDM) scheme that wavelet packet transform is utilized to change a series of parallel signals into a single composite signal. Both OFDM and WP-OFDM possess high spectral efficiency since their subcarriers are orthogonal that overlap between each other. The only difference between the two schemes is in term of the shape of the subcarriers produced. In ordinary OFDM the Fourier bases are used i.e. the sine or cosine terms. However, in WP-OFDM scheme the wavelet packet provides flexibility for modification of the filter banks property to suit the characteristic of system transmission [14]. The general multicarrier modulation system is shown in **Figure 8**.

WP-OFDM is implemented by the using the inverse orthogonal transform at the transmitter which is known as the inverse discrete wavelet packet transform (ID-WPT) as illustrated in **Figure 9** (left-hand side). The forward orthogonal transform is implemented at the receiver called as discrete wavelet packet transform (DWPT) as depicted in **Figure 9** (right-hand side). The implementation of WP-OFDM that utilizes the wavelet packet transform has been derived from MRA concept [23]. It is commenced by introducing a pair of filters called as quadrature mirror filters

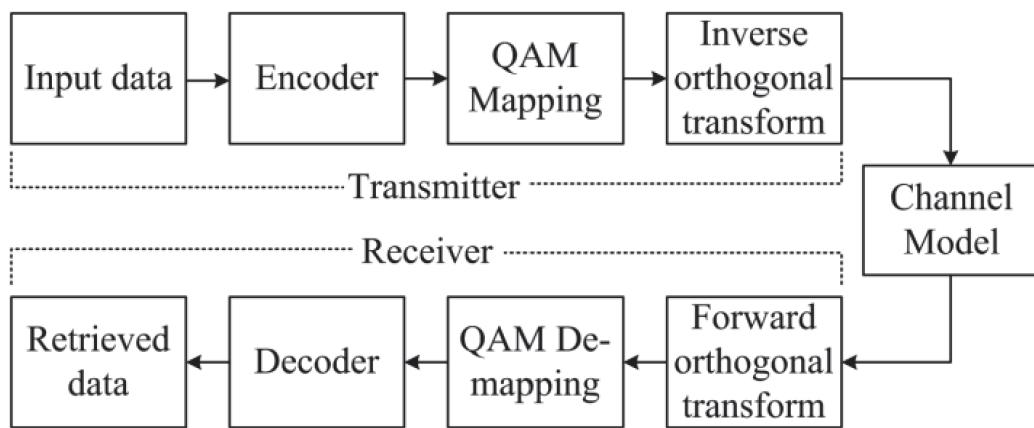


Figure 8.
General schemes for multicarrier modulation.

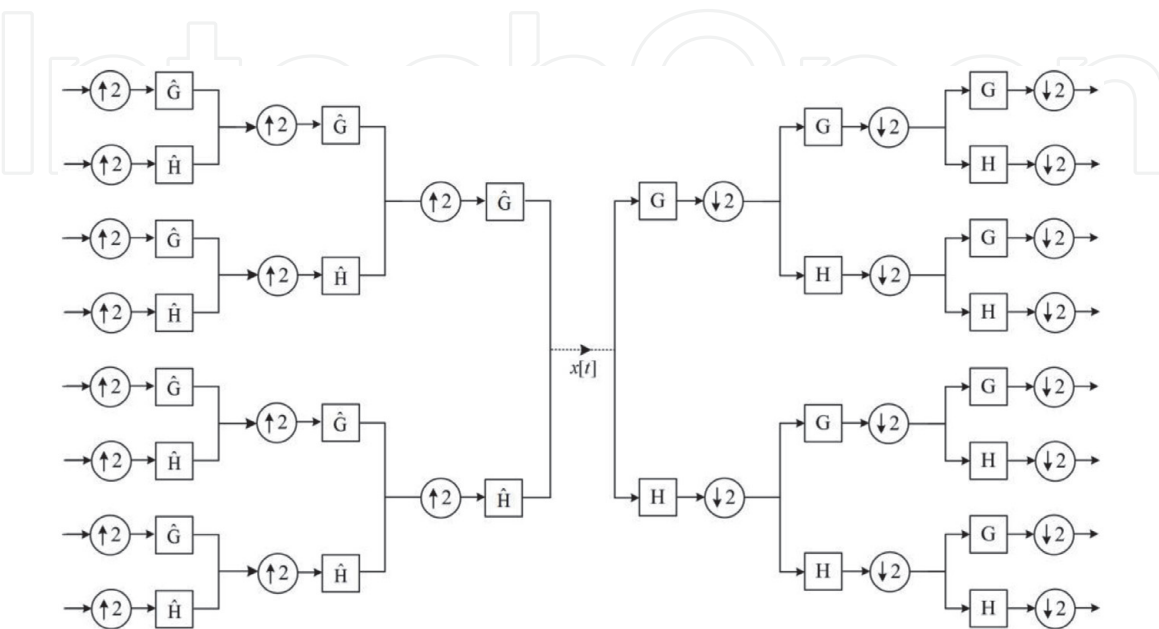


Figure 9.
IDWPT and DWPT in MCM scheme.

(QMF) that contain half-band of the low and high-pass filters, i.e. $h[n]$ and $g[n]$ respectively of length L . The relationship of the filters is described as the following;

$$g[L - 1 - n] = (-1)^n h[n] \quad (28)$$

The complex conjugate time reversed variant is given by [24];

$$h'[n] = h^*[-n] \text{ and } g'[n] = g^*[-n] \quad (29)$$

The pair of $h'[n]$ and $g'[n]$ is the synthesis filter-pair which is used to produce wavelet packet carriers for modulation at the end of the transmitter, while pair of $h[n]$ and $g[n]$ is the analysis filter-pair for demodulation at the end of the receiver. The wavelet packet coefficients Y_l^p are obtained from QMF filters which are derived via MRA as [24];

$$Y_{l+1}^{2p}(t) = \sqrt{2} \sum_m h[n] Y_l^p(2t - n) \quad (30)$$

$$Y_{l+1}^{2p+1}(t) = \sqrt{2} \sum_m g[n] Y_l^p(2t - n) \quad (31)$$

where p is subcarrier index at any tree depth l .

3. PAPR profile of wavelet-based multicarrier modulation signals

This section presents a comprehensive study on the PAPR profile of multicarrier modulation (MCM) signals. The performance of the transmitted signal is measured by the ratio of peak power signal to its corresponding average power signal within similar MCM frame, known as the peak-to-average power ratio (PAPR). It is desired to have a minimum PAPR as possible in order to reduce the complexity of high power amplifier (HPA) and at the same time, the average transmitting power can be boosted up efficiently as maximum as possible in a linear region of a HPA. Besides, it is disadvantageous of having high PAPR as the signals may be distorted in the nonlinear region of the HPA and results in poor reception and bit error rate (BER) performance. In order to cope with high PAPR, this chapter provides a study that investigates the wavelet-based OFDM (WOFDM), wavelet packet-based OFDM (WP-OFDM) and conventional OFDM systems performances. This investigation is carried out by replacing different orthogonal base modulations, which is normally used in Fourier based MCM (as the conventional OFDM system).

3.1 Multicarrier modulation system models

This section presents the general multicarrier modulation system model structures for implementation. The condition for determining the initial data value and maximum potential number of symbols to be carried by system subcarriers are also discussed.

3.1.1 System models descriptions

The three evaluated multicarrier modulation (MCM) system models are represented by a single general MCM model as illustrated in **Figure 10**. The information bits are generated based on the uniform random distribution binary

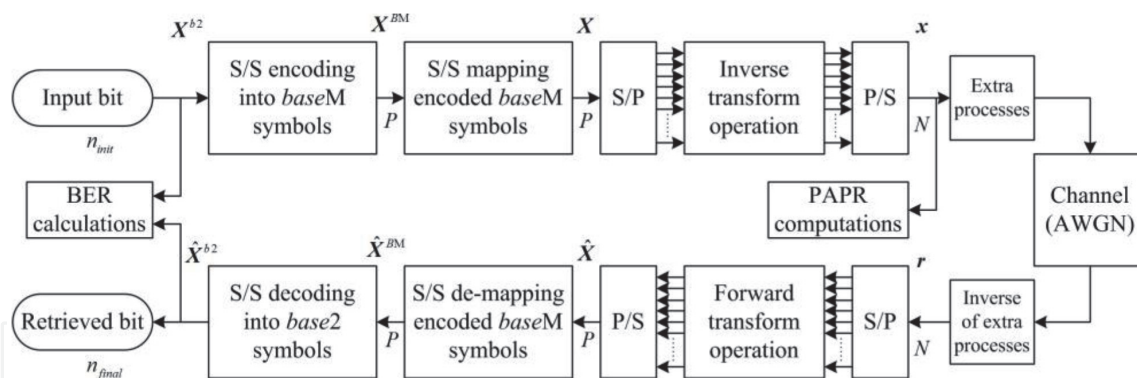


Figure 10.
Model for general MCM scheme with data sequence details.

number. The data are arranged (in every frame) in a horizontal matrix $1 \times n_{init}$, and are converted into *base16* number format. Subsequently they are encoded by Reed-Solomon (RS) codes, and converted into *baseM* number format, where M corresponds to the total mapping points in a particular QAM constellation. In this work, the Reed-Solomon of $RS(n, k)$ is used, where n is the encoded data, and k is original data. In particular, the $RS(15,11)$ is used throughout the work for protecting the original data. This channel coding scheme is compatible with hexadecimal number for encoding and decoding processes. In addition, RS encoded symbols are converted to the *baseM* symbols to achieve the same configuration that adapts with modulation constellation mapping.

Table 1 shows four possible of *baseM* number format types associated with the number of bits per symbol, N_{bps} as well as the corresponding constellation mapping modulation types. Then, the data frames are transformed into time-domain MCM signals by using a particular inverse transform prior transmission and they are retrieved back by the corresponding forward transform at the receiver. The particular inverse and forward transforms applied are labeled in block diagrams as shown in **Figures 11** and **12**.

In **Figure 11**, there are two types of wavelet-based MCM models to be considered i.e. the wavelet-based OFDM (WOFDM) and wavelet packet-based OFDM (WP-OFDM) systems. At the transmitter, either the inverse discrete wavelet transform (IDWT) or inverse discrete wavelet packet transform (IDWPT) is used. At the receiver, either the discrete wavelet transform (DWT) or discrete wavelet packet transform (DWPT) is used. These modulation techniques offer higher spectral efficiency since there is no for the system to use the cyclic pre-fix (CP) codes as in the conventional OFDM.

Figure 12 shows the conventional OFDM (C-OFDM) which is included for comparison system model. This model utilizes the inverse fast Fourier transform (IFFT) and fast Fourier transform (FFT). Additional blocks are required for appending and re-moving the CP codes where 25 percent of the OFDM frames tail are copied and appended to OFDM frames head [25, 26].

<i>BaseM</i>	No. of bits per symbol, N_{bps}	Suitable mapping type
<i>Base2</i>	1	BPSK
<i>Base4</i>	2	QAM
<i>Base16</i>	4	16QAM
<i>Base64</i>	6	64QAM

Table 1.
BaseM and its appropriate constellation mapping.

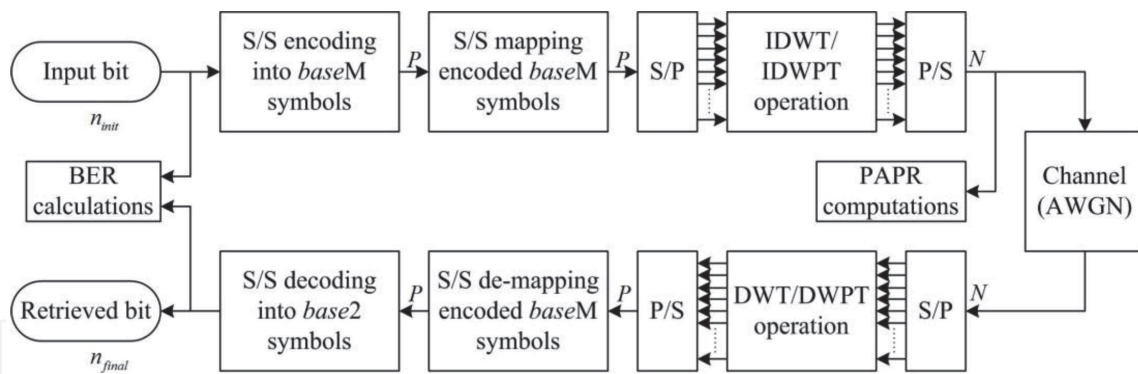


Figure 11.
 Model for wavelet- and wavelet packet-based OFDM schemes.

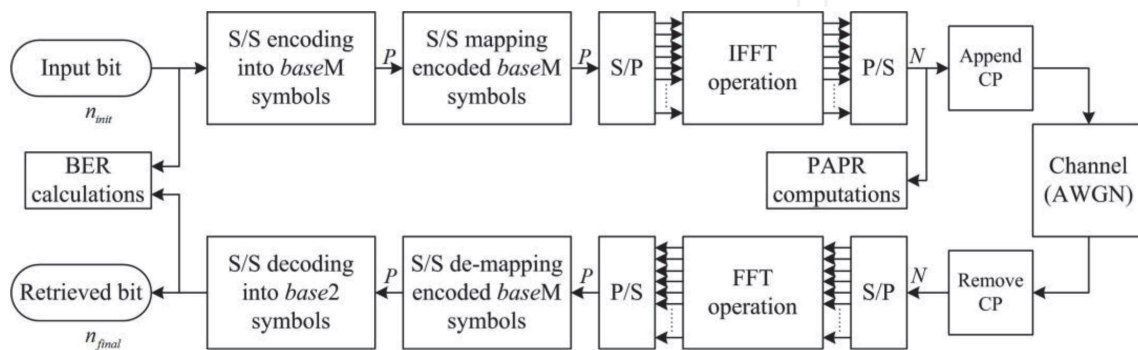


Figure 12.
 Model for conventional OFDM scheme.

Each frame must contain P symbols and is always less than or equal to the total number of subcarriers N , i.e. $P \leq N$. The specified number of base for every modulation type is fixed as in **Table 1**. The number of initial binary information n_{init} increases as the number of bits per symbol N_{bps} increased with constant value of N . In this work, the RS(15, 11) is used, and the encoded data ($n = 15$), and the original data ($k = 11$) respectively. This implies that each time a sequence of symbols to be encoded, the number of original symbols taken is eleven and this produces total fifteen encoded symbols afterwards. Therefore, during the encoding process, the raw binary data (*base2*) need to be converted to *base16* symbols to suites the requirement of RS(15, 11) coding scheme where each encoded symbol should have a value between 0 to 15.

3.1.2 Determination transmission parameter

This section describes how the transmission parameters values of P is obtained by manipulating the base number of the symbols. **Figure 10** above shows the block diagram of the of S/S encodes where raw input data bits are converted into *baseM* symbols. **Figure 13** shows further details of this process.

Figure 13 denotes three conversion processes for the initial input bit n_{init} which are indicated as the α , β and γ processes. The α process converts every four bits ($v = 4$) of binary source data to a *base16* symbol. For example, if $n_{init,base2} = \{1, 0, 0, 1, 0, 0, 1, 1, 0, 0, 1, 1, 0, 0, 1, 0, 1, 0, 0, 0, 0, 0, 0, 0, 0, 1, 1, 1, 0, 0, 0, 1, 0, 1, 1, 1, 0, 0, 1, 0, 1, 0, 0, 1\}$ then, the output from process α is $n_{\alpha} = \{9, 3, 3, 2, 8, 0, 7, 1, 7, 2, 9\}$. This means the number of overall symbols is reduced to one-fourth.

Next, β process converts every eleven *base16* symbols ($k = 11$) into fifteen *base16* encoded symbols ($n = 15$). For instance, when $n_{\alpha} = \{9, 3, 3, 2, 8, 0, 7, 1, 7, 2, 9\}$ then, the output of β process is $n_{\beta} = \{9, 3, 3, 2, 8, 0, 7, 1, 7, 2, 9, 15, 2, 7, 11\}$ which increases

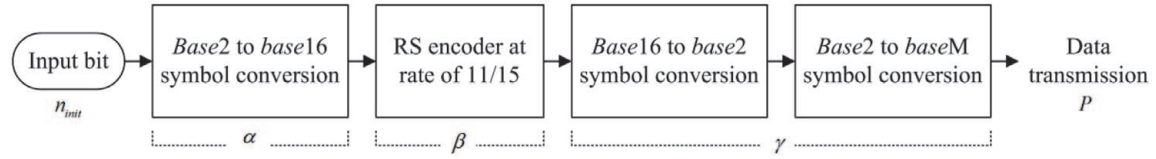


Figure 13.
S/S encoding into baseM symbols block diagram.

Mapping type	Base number	Output of γ process	Number of symbols (P) at output γ process
BPSK	Base2	$n_{\gamma,base2} = \{1,0,0,1,0,0,1,1,0,0,1,1,0,0,1,0,1,0,1,0,0,0,0,0,0,0,0,1,1,1,0,0,0,1,0,1,1,1,0,0,1,0,1,0,1,0,0,1,0,1,0,0,1,0,1,0,0,1,1,1,0,0,1,0,1,0,0,1,1,1,1,0,0,1,0,0,1,1,1,1,0,1,1\}$	60
QAM	Base4	$n_{\gamma,base4} = \{2,1,0,3,0,3,0,2,2,0,0,0,1,3,0,1,1,3,0,2,1,3,3,0,2,1,3,2,3\}$	30
16QAM	Base16	$n_{\gamma,base16} = \{9, 3, 3, 2, 8, 0, 7, 1, 7, 2, 9, 15, 2, 7, 11\}$	15
64QAM	Base64	$n_{\gamma,base64} = \{36, 51, 10, 0, 28, 23, 10, 31, 9, 59\}$	10

Table 2.
Output of γ process based on mapping type selection.

the number of symbols along the encoding processes with the additional redundancy required for channel error protection. This implies the number of overall symbols now has been increased by 15/11. After that, γ process converts every single base16 symbol into four base2 symbols ($w = 4$). Then this follows by converting every ($N_{bps} = \log_2 M$) number of base2 symbols back to a single baseM symbol. Suppose that $M = 16$, continuing the above example, when $n_\beta = \{9, 3, 3, 2, 8, 0, 7, 1, 7, 2, 9, 15, 2, 7, 11\}$ then, the output of γ process is $n_{\gamma,base16} = \{9, 3, 3, 2, 8, 0, 7, 1, 7, 2, 9, 15, 2, 7, 11\}$. The rest of other mappings are as listed in **Table 2**. The number of transmission symbols P , thus can be expressed as

$$P = n_{init} \times \left(\frac{1}{v}\right) \times \left(\frac{n}{k}\right) \times w \times \left(\frac{1}{N_{bps}}\right) \quad (32)$$

where $P \leq N$.

Using (Eq. (32)), the number of transmission symbols P and initial input bit n_{init} can be obtained after defining number of subcarriers (N). Thus, number of bits per symbol, N_{bps} can be obtained and the quantitative relationships between these parameters are shown in **Table 3**.

Figure 14 shows the partitions between the occupied slot positions of the encoded data (P) and the remaining slot positions (R) for three different values of

Parameters	Value											
No. of subcarrier, N	64			128			256					
No. of bits per symbol N_{bps}	1	2	4	6	1	2	4	6	1	2	4	6
No. of initial binary information, n_{init}	44	88	176	264	88	176	352	528	176	352	748	1100
No of symbols per frame P	60	60	60	60	120	120	120	120	250	250	250	250

Table 3.
The relationship between n_{init} , P , N and N_{bps} .

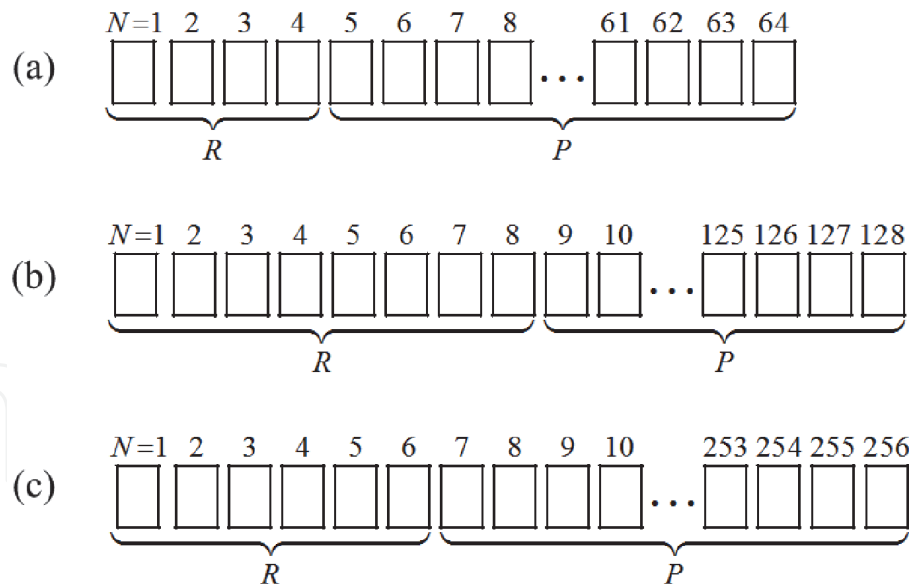


Figure 14. MCM partition with respect to N . Partition of the occupied slot: the encoded data (P) and the remaining slot positions (R) for total subcarriers $\{N = 64; 128; 256\}$.

total subcarriers $\{N = 64; 128; 256\}$. It can be observed that the subcarriers are not fully occupied for the whole slot positions with frames, hence the remaining positions, R is filled up with zeros. There are four zero frames ($N = 64$), eight zero frames ($N = 128$) and six zero frames ($N = 256$) respectively.

4. PAPR profile: results and analysis

This section presents the results and discussions on the PAPR profile performances based on several important parameters i.e. modulation types, number of subcarriers, the orthogonal bases (Fourier/Wavelets) and filter length. The BER performance is also included to investigate the efficiency of the system models. The common parameters used in the experiments are as list in **Table 4** below.

The effect of modulation constellation mapping on PAPR is analyzed in the following paragraphs. The list of parameters involved are shown as in **Table 5**. **Figure 15** shows that both the conventional C-OFDM and WP-OFDM systems are having almost the same PAPR profiles, regardless of the modulation mapping types used. The reason for the PAPR profiles of the wavelet based OFDM (WOFDM) outperform the PAPR profiles of the WP-OFDM, is that the WOFDM system contains a smaller number of signal analysis than the WP-OFDM system. The PAPR profile for WOFDM system is superior since the decomposition and reconstruction signals are only involved the low pass branches. Thus, there is lower probability for the peak to be above the average signals leading to slightly superior PAPR profile.

Parameter	Descriptions
System Model	WOFDM, WP-OFDM, C-OFDM
Encoder type	RS(15,11)
Channel model	AWGN
CP for conventional MCM	25% of total subcarriers

Table 4. Common parameters for experiments.

Parameter	Descriptions
Mapping type	QAM, 16QAM, 64QAM
Number of subcarriers	128
Orthogonal bases	Fourier, wavelet (Haar)

Table 5.
Parameters used for studying the effect of different type of mapping modulation.

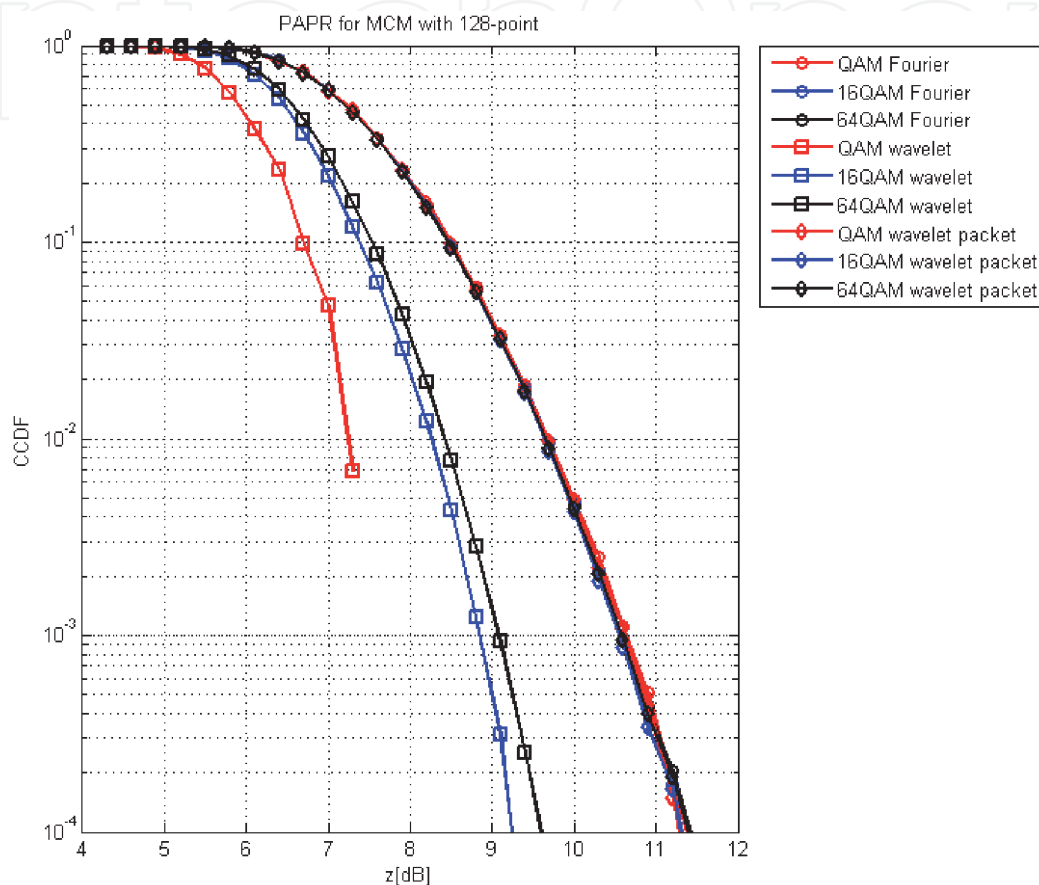


Figure 15.
CCDF of the PAPR with variation of mapping type.

However, it can clearly be seen in **Figure 16**, the BER performances are indeed worse for all three MCM systems as the type of mapping changes from QAM towards 16QAM and 64QAM. The BER performance is highly related with the type of the signal mapping used. Theoretically, the error probability at the receiver increases as the number of constellation points increased. In order to reduce the error probability, in general higher E_b/N_0 is required. **Table 6** shows for probability of bit error at 10^{-6} the corresponding of E_b/N_0 (dB) values for all modulation mapping types. The channel impairment used for evaluating the performance is using the AWGN channel. From **Figure 16**, the 64QAM modulation mapping type that can hold higher bit information, where each symbol represents 6 bits, even though it requires much higher transmitting power.

The following paragraphs analyze the effect on varying the number of subcarriers on the PAPR profiles. **Table 7** lists all parameters required for this experiment. It is found that, when the number of subcarriers N decreases i.e. from $N = 256$ until $N = 64$, the PAPR profile (CCDF) of any modulation scheme is gradually improves as shown in **Figure 17**. Explicitly, the PAPR profile of WOOFDM

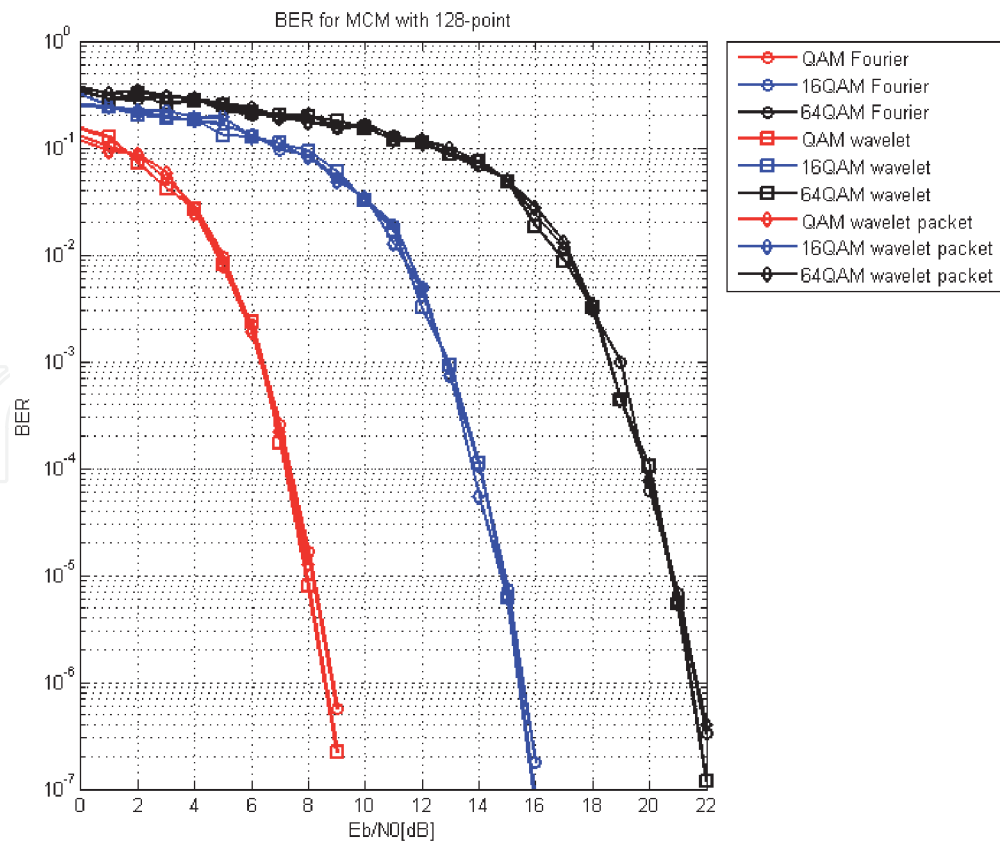


Figure 16.
 Corresponding BER performances due to variation of mapping type.

Mapping type	E_b/N_0 (dB) at BER level of 10^{-6}
QAM	9.0
16QAM	15.5
64QAM	21.5

Table 6.
 Common value of E_b/N_0 for the corresponding mapping type.

Parameter	Descriptions
Mapping type	64QAM
Number of subcarriers	64, 128, 256
Orthogonal bases	Fourier, wavelet (Haar)

Table 7.
 Parameters used for studying the effect of different No. of subcarriers.

model outperforms the PAPR profile of C-OFDM and WP-OFDM models by 1.5 dB at the CCDF level of 10^{-5} for fixed $N = 64$. The PAPR profiles for C-OFDM and WP-OFDM systems are similar. The PAPR profile for WOFDM system is superior since the decomposition and reconstruction signals are only involved the low pass branches. Thus, there is lower probability for the peak to be above the average signals leading to slightly superior PAPR profile.

Figure 18 shows that there is no significant different in term of BER performances, although different numbers of subcarriers are used for modulation. At BER of 10^{-6} , it is found that the difference between the lowest and highest value of

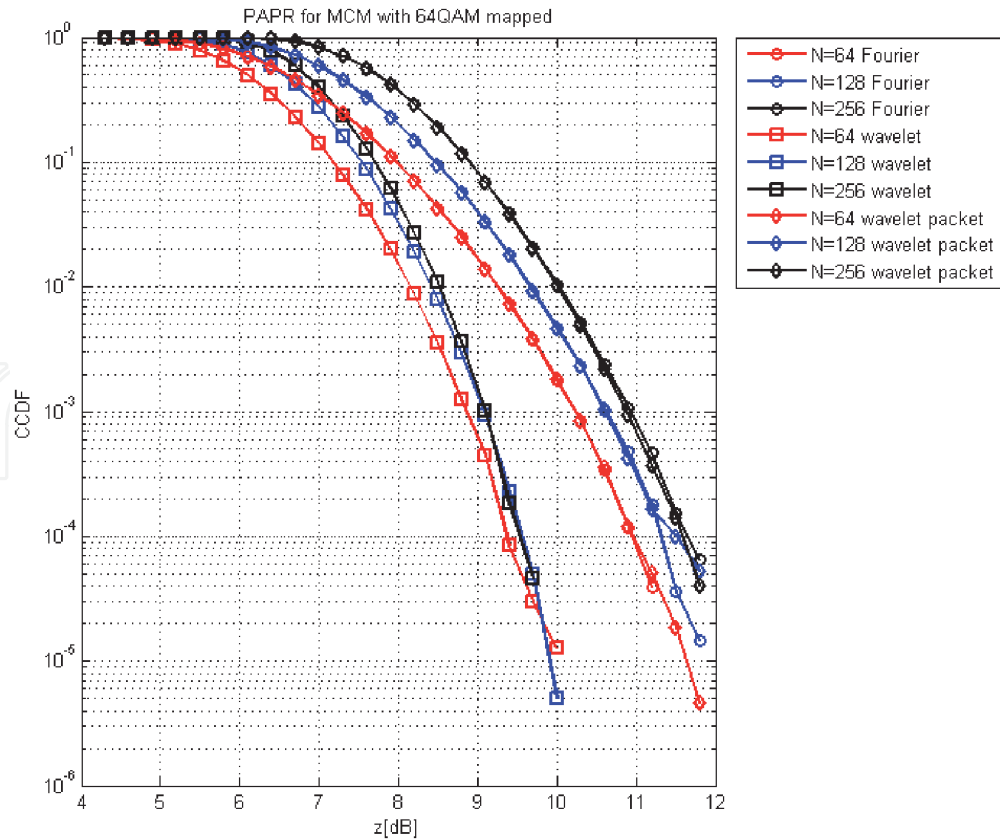


Figure 17.
CCDF of the PAPR with variation of number of subcarriers.

E_b/N_0 is less than 1 dB. Thus, it can be deduced that, the number of subcarriers gives less impact to the BER performance. The E_b/N_0 is quite high (i.e. nearly 22 dB for all profiles). The increase in the number of subcarriers worsen the PAPR profile. Therefore, for practical application, the number of subcarriers $N = 128$ is selected since it is a moderate choice as compare to the other number of subcarriers.

The following paragraphs analyze the influence of different orthogonal bases, wavelet types and their filter lengths on the PAPR profile. Several wavelet families applied includes the Daubechies, Symlet, Coiflet and Meyer wavelets with various lengths of coefficients. The parameters are briefly listed as in **Table 8**. This analysis is mainly focuses on the wavelet OFDM and wavelet packet-based OFDM systems. However, the C-OFDM scheme is also included as a performance reference. Additional information regarding the characteristic of the wavelet families are included in **Table 9**.

Figure 19 shows the PAPR profiles for the three OFDM systems, where Daubechies wavelet with different filter lengths are used (Fourier based OFDM profile is just for reference only). In analyzing the effect of wavelet filter length, various filter lengths are used in the experiment. From **Figure 19**, looking at the WOFDM profiles (red color), as the filter length increases, the PAPR profiles become worse. In other words, the Daubechies wavelet (in WOFDM) with higher filter length produces inferior PAPR profiles. This is due to the fact that with higher filter length, the wavelet has richer signal analysis. Thus, there is higher probability for the peak to be above the average signals leading to slightly inferior PAPR profile.

However, for WP-OFDM profiles (blue color), there is no significant difference in the PAPR performance. Since the signal analysis in WP-OFDM is in full binary tree analysis rather than dyadic (lower-half band) analysis in WOFDM system. There is already high amount of data involved in decomposition and reconstruction which makes the effect of wavelet filter length insignificant.

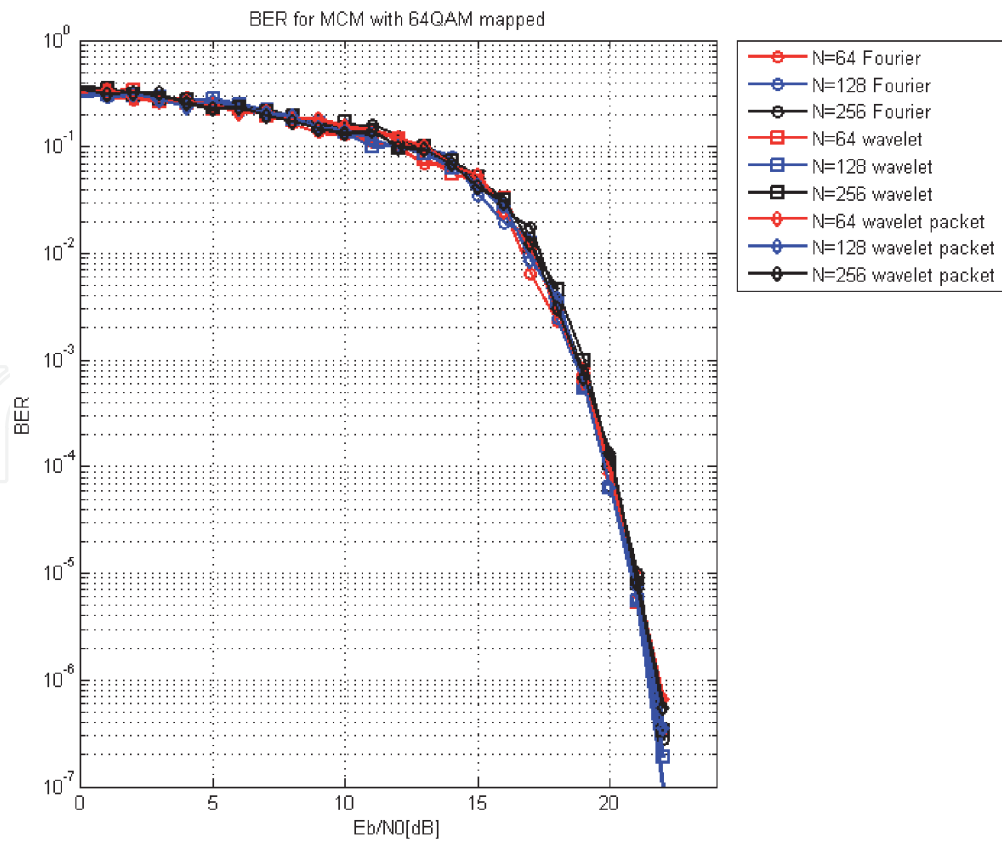


Figure 18.
 Corresponding BER performance due to variation of number of subcarriers.

Parameter	Descriptions
Mapping type	64QAM
Number of subcarriers	128
Orthogonal bases	Fourier, wavelet (<i>db1, db2, db3, db5, db10, db20, sym2, sym3, sym5, sym10, coif1, coif3, coif5, dmey</i>)

Table 8.
 Parameters used for studying the effect of different bases and filter length.

Full name	Abbreviated name	Vanishing order	Length, L
Haar	Haar	1	2
Daubechies	<i>dbN</i>	N	$2N$
Symlets	<i>symN</i>	N	$2N$
Coiflet	<i>coifN</i>	N	$6N$
Discrete Meyer	<i>dmey</i>	—	62

Table 9.
 Wavelet family characteristic [23].

In **Figures 20** and **21**, different wavelet types (Daubechies, Symlet, Coiflet and Discrete Meyer wavelets) are used but the filter length is fixed $L = 6$ (short category). For long category the filter lengths are mixed, i.e. $L = \{18(\text{coif } 3), 20(\text{db}10, \text{sym}10), 62(\text{dmey})\}$ respectively. From these figures, there can be observed

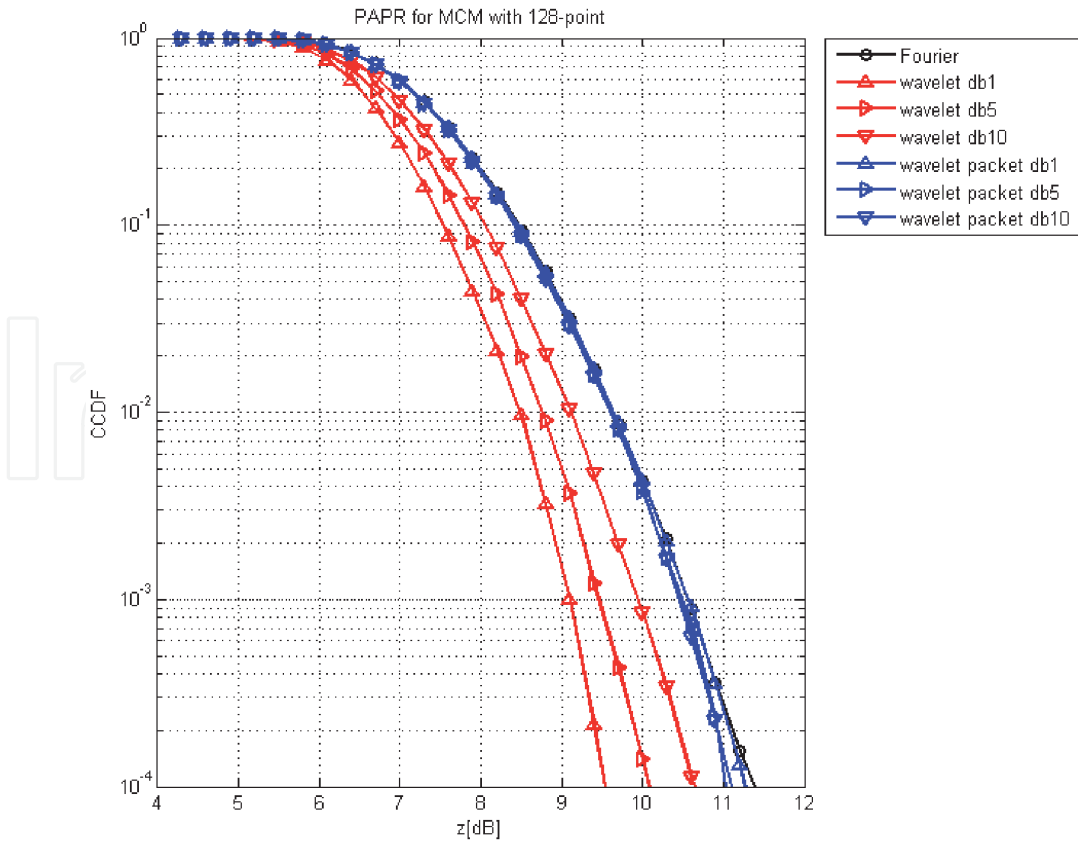


Figure 19.
CCDF of the PAPR with Daubechies wavelet with different filter lengths.

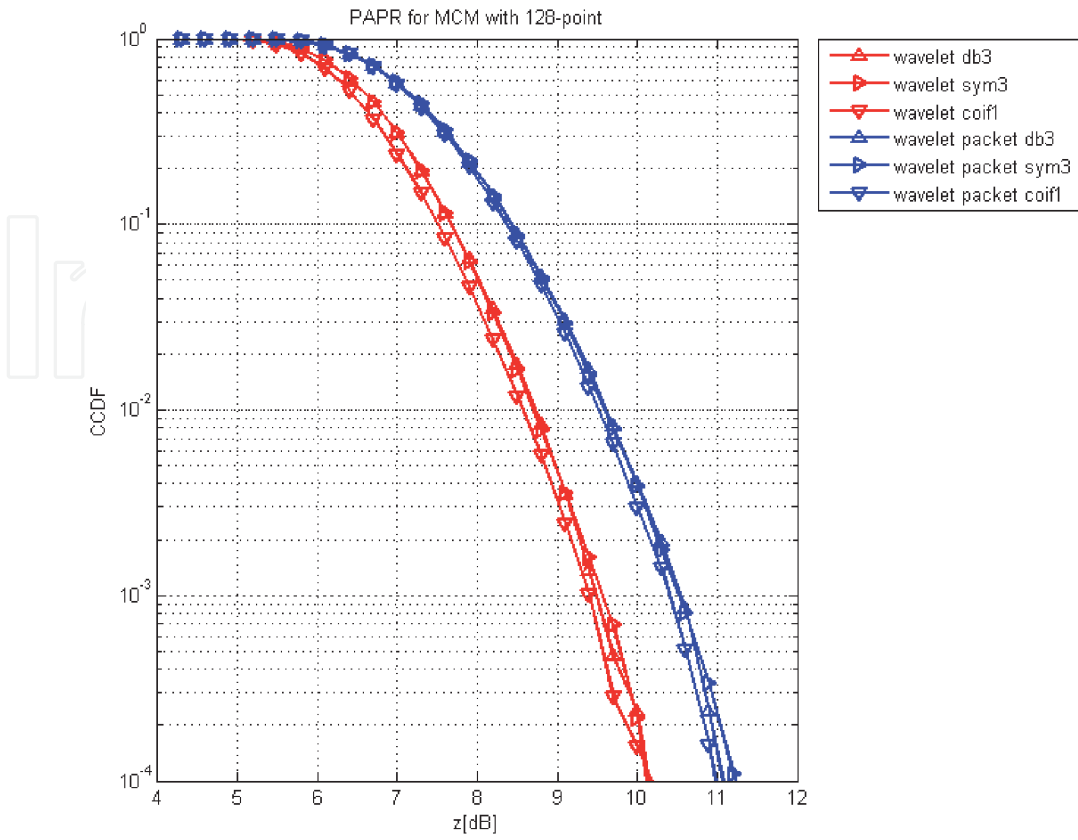


Figure 20.
CCDF of the PAPR with different orthogonal bases modulation and *short* filter lengths.

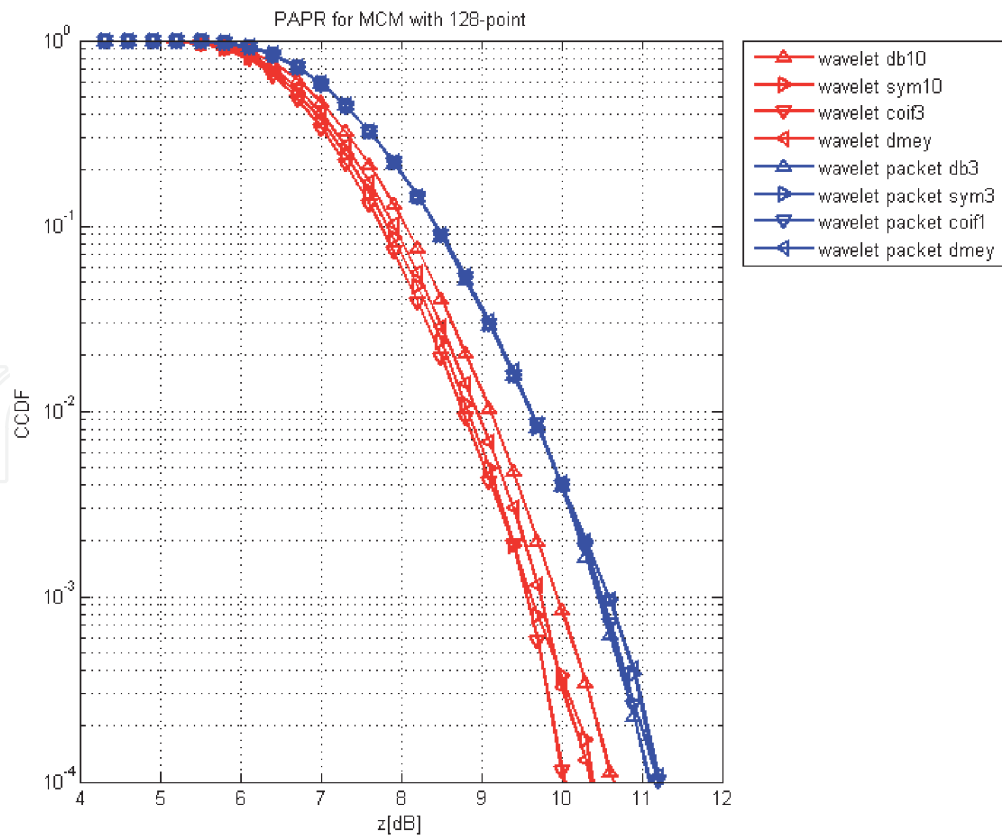


Figure 21. CCDF of the PAPR with different orthogonal bases modulation and long filter lengths.

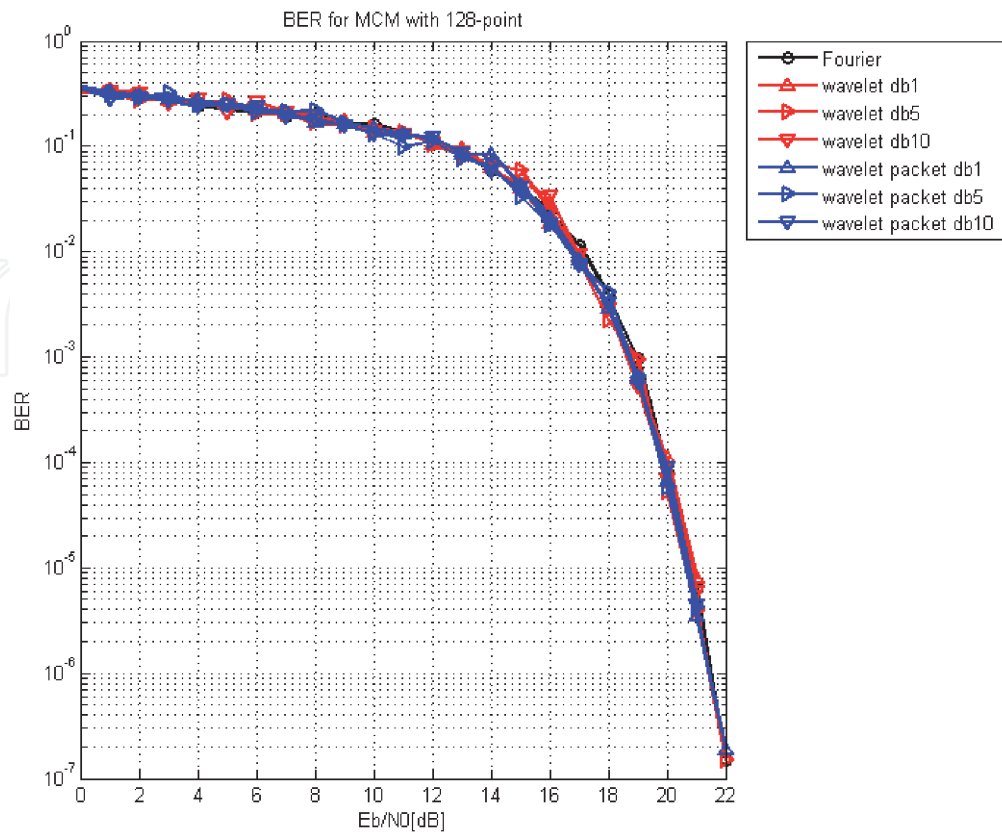


Figure 22. Corresponding BER performances for Daubechies wavelet with different filter lengths.

that no explicit difference found from PAPR profiles of WP-OFDM signals either by changing the wavelet's type or length.

The BER performances are shown in **Figure 22**, where the experiment is carried out on the Daubechies wavelet with different filter lengths. It can be observed that no significant difference between BER performances. For example, at BER 10^{-6} all profiles having the same value of E_b/N_0 .

5. Conclusion

The phenomenon of high PAPR in MCM system cannot be avoided since the signals consist of multiple low-rate parallel signals, which can be seen as the composite subcarriers in time domain representation. It is expected by using different orthogonal base for modulation, the PAPR profile can be reduced. Hence, discrete wavelet transform (DWT) and discrete wavelet packet transform (DWPT) are used for this purpose instead of fast Fourier transform (FFT). In comparison to the C-OFDM system, WOFDM and WP-OFDM systems do not need any cyclic prefix (CP) codes for their MCM frame in order to avoid intercarrier interference (ICI) and inter symbol interference (ISI).

Although, WOFDM system provides superior PAPR performance than other systems, data are lost at higher frequencies branches since signals decomposition are in dyadic (lower half-band) fashion. On the other hand, WP-OFDM system decomposes the signals in both lower and upper-band frequencies, that enrich signals analysis. The results obtained in Section 4 proves the characteristics. In addition, applying various wavelet bases do not offer much improvement in PAPR profile.

Acknowledgements


The authors would like to acknowledge the USM RU grant (Grant No. 1001/PELECT/814100), for funding this research work.

Author details

Jamaluddin Zakaria and Mohd Fadzli Mohd Salleh*
School of Electrical and Electronic Engineering, Universiti Sains Malaysia,
Seri Ampangan, 14300 Nibong Tebal, Pulau Pinang, Malaysia

*Address all correspondence to: fadzlisalleh@usm.my

IntechOpen

© 2020 The Author(s). Licensee IntechOpen. This chapter is distributed under the terms of the Creative Commons Attribution License (<http://creativecommons.org/licenses/by/3.0>), which permits unrestricted use, distribution, and reproduction in any medium, provided the original work is properly cited. 

References

- [1] Van Nee R, Prasad R. OFDM for Wireless Multimedia Communications. Boston, London: Artech House; 2000.
- [2] Zakaria J, Salleh M. F. M. Wavelet-based OFDM analysis: BER performance and PAPR profile for various wavelets. In: Proceedings of the IEEE Symposium on Industrial Electronics and Applications (ISIEA '12); 23–26 September 2012; Bandung, Indonesia: IEEE; 2012. P. 29–33.
- [3] Chafii M, Palicot J, Gribonval R, Burr A. G. Power spectral density limitations of the wavelet-OFDM system. In: Proceedings of the 24th European Signal Processing Conference (EUSIPCO 16); 28 August-2 September 2016; Budapest, Hungary: 2016. P. 1428–1432, doi: 10.1109/EUSIPCO.2016.7760484.
- [4] Hsu C. Y., Liao, H. C. Generalised precoding method for PAPR reduction with low complexity in OFDM systems. IET Communications. 2018; 12 (7): 796–808. DOI: 10.1049/iet-com.2017.0824
- [5] Kaur J, Sharma V. A-STBC incorporated power-efficient Radio over Fibre system, Optics Communications. 2019; 441: 84–89.
- [6] Sarowa S, Kumar N, Agrawal, Balwinder S S. Evolution of PAPR Reduction Techniques: A Wavelet Based OFDM Approach, Wireless Personal Communications. 2020; <https://doi.org/10.1007/s11277-020-07643-1>
- [7] Muller S, Huber J. A Comparison of Peak Power Reduction Schemes for OFDM. In: Proceedings of the IEEE Global Telecommunications Conference (GLOBECOM '97), 3–8 Nov. 1997; Phoenix, Arizona: 1, P. 1–5.
- [8] Bouhleb A, Sakly A, Mansouri M. N. Partial Transmit Sequence technique based on Particle Swarm Optimization for WOFDM PAPR reduction. In: Proceeding of the 2nd International Conference on Advanced Technologies for Signal and Image Processing (ATSIP '16), March 21–23, 2016; Monastir, Tunisia: P. 710–714, doi: 10.1109/ATSIP.2016.7523183.
- [9] Zakaria J, Salleh, M. F. M. PAPR reduction scheme: wavelet packet-based PTS with embedded side information data scheme. IET Communications. 2017; 11 (1), 127–135
- [10] Yoon E, Hwang D, Jang C, Kim J, Yun U. Blind Selected Mapping with Side Information Estimation Based on the Received Pilot Signal, Wireless Communications and Mobile Computing. 2018; (5):1–9, DOI: 10.1155/2018/8523680
- [11] Ahmed M S, Boussakta S, Al-Dweik A, Sharif B, Tsimenidis C C. Efficient Design of Selective Mapping and Partial Transmit Sequence Using T-OFDM. IEEE Transactions on Vehicular Technology. 2020; 69(3), 2636–2648, doi: 10.1109/TVT.2019.2928361.
- [12] Daubechies I. Ten Lectures on Wavelets. Society for Industrial and Applied Mathematics. 1992. doi.org/10.1137/1.9781611970104
- [13] Li A, Shieh W, and Tucker R. Wavelet Packet Transform-Based OFDM for Optical Communications, Journal of Lightwave Technology. 2010; 28(24): 3519–3528.
- [14] Torun B. Peak-to-Average Power Ratio Reduction Techniques for Wavelet Packet Modulation. PhD thesis, Microwave Technology and Systems for Radar (MTSR), Department of Telecommunications, Faculty of Electrical Engineering, Mathematics and Computer Science, Delft University of Technology. 2010.

- [15] Gargour C, Gabrea M, Ramachandran V, Lina J M. A Short Introduction to Wavelets and Their Applications, IEEE Circuits and Systems Magazine. 2009; 9(2): 57–68.
- [16] Burrus S C, Gopinath R A, Guo H. Introduction to Wavelets and Wavelet Transforms: A Primer. Prentice Hall. 1997.
- [17] Akansu A N, Haddad R A. Multiresolution Signal Decomposition: Transforms, Subbands, and Wavelets. Academic Press, Inc., Orlando, FL, USA. 1992.
- [18] Mallat S G. Multiresolution Approximations and Wavelet Orthonormal Bases of $L^2(R)$, Transactions of the American Mathematical Society. 1989; 315(1): 69–87.
- [19] Li A, Shieh W, Tucker R. Wavelet Packet Transform-Based OFDM for Optical Communications, Journal of Lightwave Technology. 2010; 28(24): 3519–3528.
- [20] Goswami J C, Chan A K. Fundamentals of Wavelets: Theory, Algorithms, and Applications, Second Edition, John Wiley & Sons, Inc; 2011.
- [21] Chang R W. Synthesis of Band-Limited Orthogonal Signals for Multichannel Data Transmission, Bell Systems Technical Journal. 45: 1775–1796. see also U.S. Patent 3,488,445, Jan. 6, 1970.
- [22] Erdol N, Bao F, Chen Z. Wavelet Modulation: A Prototype for Digital Communication Systems. In: Proceeding of the IEEE Conference Record Southcon '95, 7–9 March, Fort Lauderdale, FL: 1995. P. 168–171.
- [23] Jamin A, Mähönen P. Wavelet Packet Modulation for Wireless Communications: Research Articles, Wireless Communications and Mobile Computing. 2005; 5(2): 123–137.
- [24] Vetterli M, Kovacevic J. Wavelets and Subband Coding, Prentice Hall Signal Processing Series, Prentice Hall PTR. 1995.
- [25] Jr R M W. IEEE 802.16 Broadband Wireless Access Working Group. Technical report. SciCom, Inc. 2001.
- [26] Zhang L. A Study of IEEE 802.16a OFDM-PHY Baseband. Master's thesis, Department of Electrical Engineering, Linköping Institute of Technology. 2005